RF PERFORMANCE RESULTS OF THE 2nd ELBE SRF GUN

A. Arnold#, M. Freitag, P. Murcek, J. Teichert, H. Vennekate, R. Xiang, HZDR, Dresden, Germany
P. Kneisel, G. Ciovati, L. Turlington, JLAB, Newport News, USA

Abstract

An improved SRF gun (ELBE SRF Gun II) has been installed and commissioned at HZDR. This new gun replaced the first SRF gun of the ELBE accelerator which had been in operation since 2007. The new gun has an improved 3.5-cell niobium cavity those SRF performances have been studied first with a copper cathode. After the replacement by our standard Cs_2Te-cathode we observed a tremendous degradation of the cavity gradient paired with an increase of field emission.

In this contribution we will report on our in-situ investigations to find the origin and the reason for the particle contamination that happened during the first cathode transfer.

INTRODUCTION

At the superconducting (SC) electron linear accelerator of the ELBE radiation facility [1] a new superconducting electron photo injector has been installed in May 2014. This SRF gun II is replacing the previous one which had been in successful operation from 2007 until April 2014. Although SRF gun I could not reach the design specifications, it was successfully operated for R&D purposes and also some dedicated user experiments at the ELBE accelerator had been done [2].

For SRF gun II a new niobium cavity has been built, treated and tested at JLab [3]. At the same time a new cryomodule has been designed and built at HZDR [4]. In November 2013, the cavity was shipped to HZDR and assembled into the cryomodule. About half a year later, the gun was installed into the ELBE accelerator hall and since June 2014 it is under commissioning for beam tests.

The main goal of SRF gun II is to achieve medium average current (1 mA) and low emittance (1 mm mrad) at a moderate bunch charge (77 pC) as well as to test new semiconductor cathodes.

COLD MASS DESIGN

The design of the cold mass is shown in Figure 1. Most of the components are identical to the previous SRF gun I [5]. The 1.3 GHz Nb cavity, for example, consists of three TESLA like cells and a specially designed half-cell. The latter got improved stiffening and a slightly stronger electric field distribution (80% of the on-axis field in the three TESLA like cells). Another superconducting cell, called choke filter, is surrounding the cathode and prevents RF leakage into the cathode support system.

The photocathode itself is isolated from the cavity by a vacuum gap and cooled down with liquid nitrogen. Both allow the application of a normal conducting (NC) photocathodes with high quantum efficiency (QE) such as Cs_2Te or GaAs.

New is the integration of a SC solenoid in the cryomodule. Compared to the NC solenoid of SRF gun I, which was placed downstream the gun, the new design is much more compact and the distance to the cathode is smaller. The SC solenoid is placed on a remote-controlled x-y table to align its center to the electron beam axis. Additional µ-metal shields hold the solenoid remanence field as well as the field of the stepper motors on a 1 µT level near the cavity. Details of the SC solenoid design and testing are published in [6].

Q_0 vs. E_{ACC}

In order to evaluate the performance of the cavity it is most common to measure the intrinsic quality as a function of the accelerating gradient. For a strongly over coupled cavity, both quantities can be determined by the dissipated and transmitted power (P_{diss} and P_t) as well as by the external quality factor of the fundamental pickup Q_t and the normalized impedance r_s = 165 Ohm (see eq.(1)). The cavity length is L = 0.5 m.

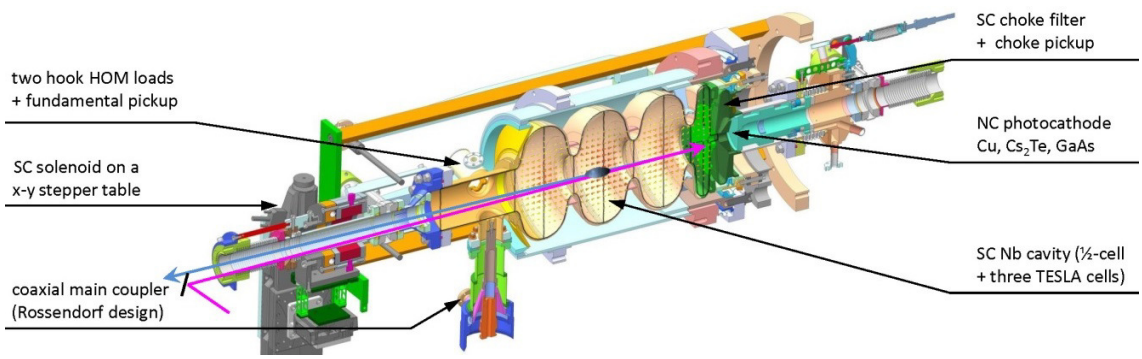

Figure 1: 3D drawing of the ELBE SRF gun II cold mass.

#a.arnold@hzdr.de

ISBN 978-3-95450-178-6

$$E_{acc} = \frac{1}{L}\sqrt{2 r_s Q_t P_t} \quad \text{and} \quad Q_0 = \frac{Q_t P_t}{P_{diss}} \qquad (1)$$

The performance has been measured vertically after preparation as well as horizontally later in the SRF gun cryomodule with a copper and a Cs_2Te cathode. As shown in Figure 2, the cavity lost about 30% of its performance compared to the last vertical test and got even worse after the first Cs_2Te- cathode exchange. Although the remaining gradient is still higher than that of SRF gun I, this was a bitter setback that demonstrates the high risk of placing NC cathodes in SC cavities.

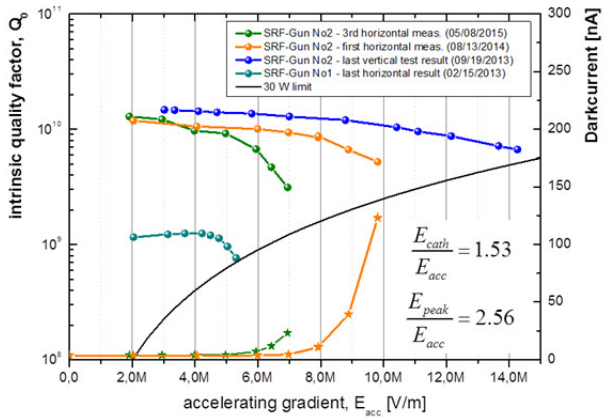

Figure 2: Intrinsic quality factor as a function of the accelerating gradient; also in comparison to SRF gun I.

SPATIAL RADIATION DISTRIBUTION

The first try to get more information about the reason and the origin of the cavity contamination was to measure the spatial distribution of the radiation caused by field emitted (FE) electrons. Therefore, 40 optically stimulated luminescence (OSL) dosimeters have been attached around the cryostat as shown in Figure 3 (8 at the circumference of each cavity cell, 4 on the front and 4 on the back plane).

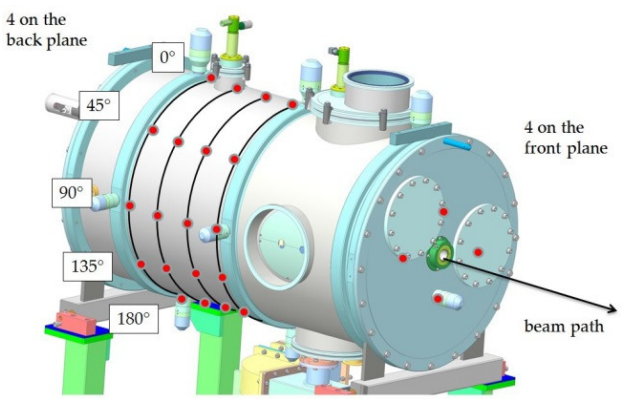

Figure 3: Position of 40 OSL dosimeters to measure the radiation distribution caused by field emitted electrons.

The dosimeters have being exposed for 90 min at the maximum achievable cavity gradient of 7.1 MV/m. The resulting radiation distribution is shown in Figure 4.

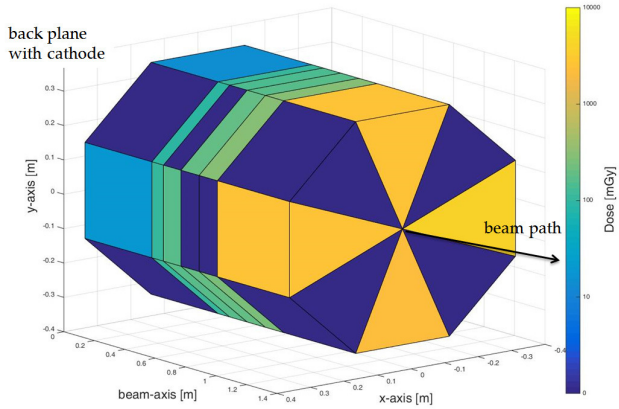

Figure 4: Radiation distribution (dose) at the cryo module after a 90 min exposure at E_{acc}=7.1 MV/m.

Obviously, the FE electrons produce a radiation cone that is directed to the downstream direction and thus it is most likely that these electrons are originated somewhere in the first (half) cell of the cavity (see Figure 1).

Q_0 vs. E_{PEAK} FOR ALL MODES

To get closer to the origin of the limiting cell, it is common to determine the Q_0 vs. E_{peak} for all passband modes. This is typically done by calculating the stored energy U based on the measured forward or transmitted power (P_i, P_t) as well as on the bandwidth BW, the external Q_t and the frequency f_0 of each mode (Table 1).

$$U = \frac{2P_i}{\pi BW} \quad \text{or} \quad U = \frac{Q_t P_t}{2\pi f_0} \qquad (2)$$

Table 1: Important Properties of the Passband Modes.

	¼ π	½ π	¾ π	π
f_0 [MHz]	1267.677	1282.792	1294.764	1300.000
BW [Hz]	2.3	133	272	145
Q_t	1.91E13	2.94E11	1.424E11	2.58E11

Once the energy is known, the peak electric field in each cell and for each mode simply follows from the corresponding proportional constants (Table 2) simulated by an electromagnetic code (Figure 5)

$$E_{\text{cell}}^{\text{mode}} = k_{\text{cell}}^{\text{mode}}\sqrt{U}; \quad \left[k_{\text{cell}}^{\text{mode}}\right] = (\text{MV/m})\,\text{J}^{-1/2}. \qquad (3)$$

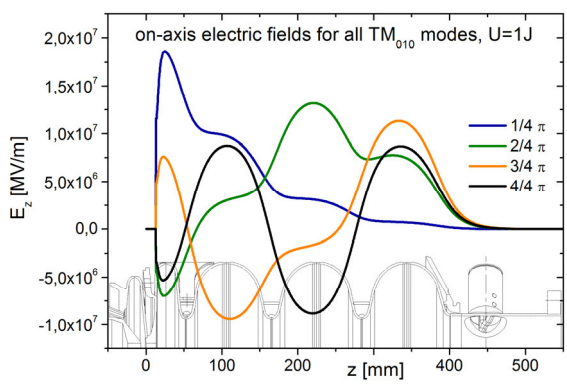

Figure 5: On-axis fields to determine $k_{\text{cell}}^{\text{mode}}$ for all modes.

Table 2: Proportional Constants for all our Modes in the Middle of each Cell; the Unit is $\left[k_{\text{cell}}^{\text{mode}}\right] = (\text{MV/m})\,\text{J}^{-1/2}$

$k_{\text{cell}}^{\text{mode}}$	¼ π	½ π	¾ π	π
halfcell	15.6759	-7.2597	9.1671	6.6701
TESLA 1	12.4326	0.726	-8.0101	-8.4659
TESLA 2	4.7568	13.1581	-3.382	8.808
TESLA 3	0.1081	8.6208	11.3921	-8.4659

Finally, by adding the dissipated power P_{diss}, which is determined by an electric heater in the helium bath, one gets the intrinsic quality factor by

$$Q_0 = \frac{f_0}{BW}\frac{4P_i}{P_d} \quad \text{or} \quad Q_0 = \frac{Q_t P_t}{P_d} \ . \qquad (4)$$

The Q_0 vs. E_{peak} is now evaluated for an on-axis peak field in the middle of each cell and for each mode. This creates four diagrams with four curves each. The idea is now to observe similar trends for each mode in the same cell. If different modes with different field distributions are limited to the same electric field it is very likely that the electron emitting particle is the same for all these modes. And indeed this behaviour could be found for the first TESLA like cell, while all other cells do not show any similarity (Figure 6).

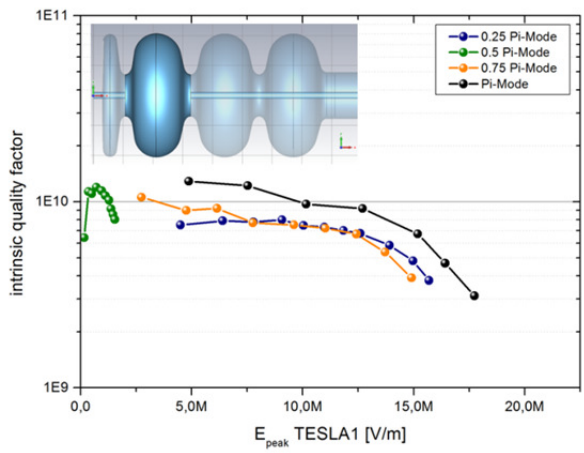

Figure 6: Q_0 vs. E_{peak} for all four passband modes in the first TESLA like cell.

DARK CURRENT ANALYSIS

To get even closer to the field emitter, we finally measured the energy spectrum of the escaping dark current electrons in the downstream diagnostic beamline. As shown in Figure 7 the main contributor has an energy of 2.8 MeV, which is 0.8 MeV below the energy of the photo emitted electrons and thus the emitter is most likely not at the backplane of the half cell.

To identify its exact origin, the measured energy spectra are compared with CST PIC simulations [7] where the electron emission points are swept along the z-axis over the inner surface of the first TESLA cell. The emission phase was chosen between ±45° around the crest, which realizes a phase scan at highest surface fields. The electrons as well as those properties are finally determined by a particle monitor at the cavity exit. Basically, we are concentrating only on both irises of the first TESLA cell because these are regions with highest electric fields.

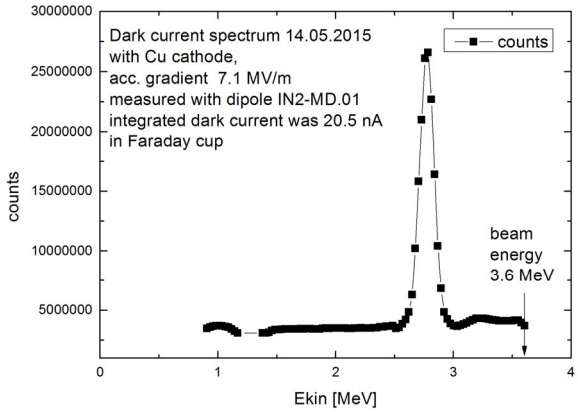

Figure 7: Energy spectrum of dark current electrons emitted at E_{acc} = 7.1 MV/m and measured in the downstream diagnostics beamline.

As a result, it was found that only a small zone of 3 mm at the first iris (btw. 24th and 26th mm along the z-axis) emits electrons having the right energy of 2.8 MeV (Figure 8 and Figure 9). For all other emission points the energy is lower or the electrons cannot even escape.

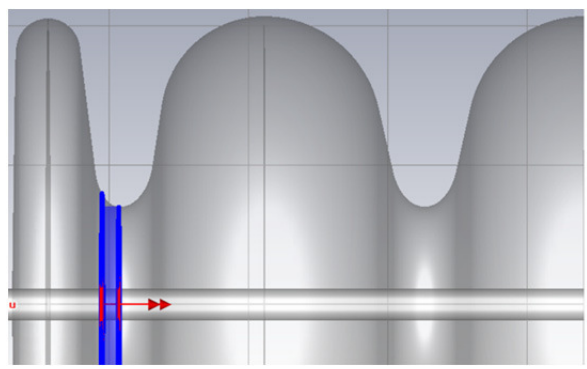

Figure 8: Most likely position of the field emitter.

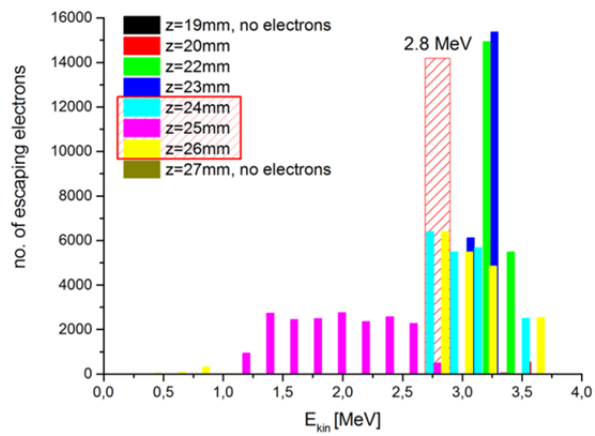

Figure 9: Simulated energy spectra of the escaping electrons for different emission points along the z-axis.

ISBN 978-3-95450-178-6

CONCLUSION

Although the results of the first commissioning period of SRF gun II have been very promising [8], we had to except a bitter setback after the first cathode exchange. We observed a serious contamination that was very likely caused by a particle moved from cathode surface to first iris of the cavity. By optical inspection with a microscope we found such a smoking gun at the surface of the cathode (Figure 10) and even scratches have been observed that might be responsible for the degradation as well.

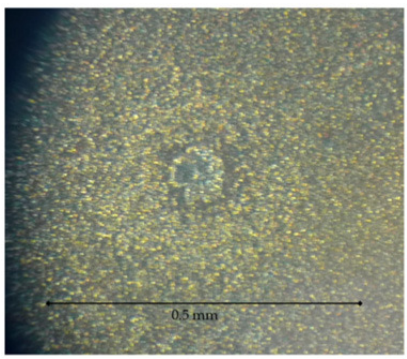

Figure 10: Crater of an exploded particle at the cathode surface, probably the smoking gun of the degradation.

Based on these observations the risk of SRF gun cavities by NC cathodes is not eliminated, yet! More efforts have to be made to avoid any particles created by the semiconductor, the transfer mechanism or the cathode substrate itself.

ACKNOWLEDGMENT

We are greatly indebted to Peter Kneisel, who mainly realized the fabrication and preparation of the cavity. We also like to thank our colleagues at JLab and HZDR, who supported this work. Finally, we acknowledge the support of the European Research Infrastructure Activity under the FP7 programme (EuCARD-2, contract number 312453 and LA3NET, contract number 289191) as well as the support of the German Federal Ministry of Education and Research grant 05K12CR1.

REFERENCES

[1] P. Michel, “The radiation source ELBE at the Forschungszentrum Dresden-Rossendorf”, Nuclear Science Symposium Conference Record, 2008. NSS '08, IEEE, pp. 3078 (2008).

[2] J. Teichert, et al., Nuclear Instruments and Methods in Physics Research A 743 (2014) 114-120.

[3] A. Arnold, et al., “Fabrication, Tuning, Treatment and Testing of Two 3.5 Cell Photo-Injector Cavities for the ELBE Linac”, TUPO019, Proc. 15th Int. Conf. on RF Superconductivity, Chicago, USA (2011).

[4] P. Murcek, et al., “The SRF Photoinjector at ELBE – Design and Status 2013”, MOP025, Proc. 16th Int. Conf. on RF Superconductivity, Paris, France (2013).

[5] A. Arnold, et al., Nuclear Instruments and Methods A 577 (2007) 440.

[6] H. Vennekate, et al., “Emittance Compensation for an SRF Photo Injector”, MOP026, Proc. 16th Int. Conf. on RF Superconductivity, Paris, France (2013).

[7] CST - Computer Simulation Technology AG: CST GmbH, 64289 Darmstadt, Germany, http://www.cst.com

[8] J. Teichert, et al., “Commissioning of an Improved Superconducting RF Photo Injector at ELBE”, THP061, Proc. 36th Int. Free Electron Laser Conf., Basel, Switzerland (2014).